AN ANALYSIS OF HEATING UNIFORMITY IN WOOD HIGH-FREQUENCY DRYING

Hao-Jie Chai
Doctoral Candidate
E-mail: nefuchj@163.com

Jing-Yao Zhao
Doctoral Candidate
E-mail: zjy_29445629@qq.com

*Ying-Chun Cai**
Professor of Wood Science and Technology
Key Laboratory of Bio-Based Material Science and Technology
College of Material Science and Engineering
Northeast Forestry University
Harbin, People's Republic of China
E-mail: ychcai@aliyun.com

(Received March 2018)

Abstract. The high-frequency heating temperature field simulation model was built using finite element method and validated by experiments. Under the premise of ensuring model accuracy, the model parameters (plate spacing and area, wood dielectric constant, stack length and width, and heating time) were individually varied to assess the impact of these parameters on wood heating uniformity. The results showed the following: 1) The model has good accuracy as verified by experiments. 2) In the thickness direction, the middle layer temperature was higher than the upper and lower surface temperatures; in the length and width directions, the center temperature was lower than those of both ends and both sides, and the temperature at the corners was the highest. 3) The smaller the distance between the plates, the better the heating uniformity; with the plate area increasing, the heating uniformity first increased and then decreased; the smaller the wood dielectric constant, the better the heating uniformity; as the continuous heating time increased, the heating uniformity first decreased, then increased, and then again decreased; as the length and width of the stack increased, the heating uniformity decreased first, then increased, and then again decreased; when they were the same size as the plate, the heating uniformity was the best.

Keywords: High-frequency heating, wood drying, simulation model, heating uniformity.

INTRODUCTION

As the demand for large-section drying and high-quality square timber is increasing (Guo et al 2009), the high-quality, rapid, and energy-saving drying technologies are gaining increased worldwide attention from scholars and engineers (Lv et al 2015). High-frequency vacuum drying is a combined drying technology which combines the advantages of high-frequency heating and vacuum drying and is an ideal drying method for precious wood species, wooden handicrafts, and large-section timber of good permeability (Ai 2016). The wood temperature distribution not only affects the drying speed of wood, but also affects the drying quality (Xiao 2009). However, it has been difficult to ensure the uniformity of internal temperature distribution of wood during high-frequency heating which caused a big hurdle in wood high-frequency vacuum drying. Therefore, it is of great significance to study the uniformity of wood temperature distribution during high-frequency drying.

Cai et al (2001) systematically studied the high-frequency vacuum drying mechanism quantitatively and qualitatively. Lee et al (2010) studied

* Corresponding author

Wood and Fiber Science, 50(3), 2018, pp. 337-345
https://doi.org/10.22382/wfs-2018-032

the effects of high temperature, low humidity, and incisions on the high-frequency vacuum drying characteristics of 150 mm × 150 mm × 3500 mm Japanese cedar with pith. Huang et al (2013) took Chinese fir as the research object, and explored the effects of wood MC, thickness, and high-frequency power on the heating rate. Wang (2013) experimentally studied the drying mechanism of the high-frequency vacuum drying process of Japanese cedar, and analyzed that high frequency-vacuum drying had obvious advantages over conventional drying; and a high-frequency vacuum drying model of wood was established based on BP (Back Propagation) neural network. Jia (2015) systematically studied the heat and mass transfer mechanism of the timber with pith in the high-frequency vacuum drying process along the fiber direction, and established a one-dimensional mathematical model of heat and mass transfer. Rabidin et al (2017) used 30-mm and 50-mm-thick kekatong as the research object and compared the drying characteristics of the tree under high-frequency vacuum and conventional drying by experiments. Liu et al (2017) studied large-scale European Pinus densiflora as the research object, and compared and analyzed the MC distribution, color change, and cracking of the dried wood after vacuum setting/vacuum high-frequency drying and high temperature setting/high temperature drying. At present, the researchers at home and abroad mainly focus on the mechanism and technology datum of high-frequency drying. Wood is a heterogeneous organic organism with large variability (Li et al 2012). The temperature distribution inside wood and associated mechanism are very complicated during the high-frequency heating and drying process, and a mathematical model could intuitively reflect the heat transfer mechanism of wood in the drying process (Zhao et al 2015a,b). However, the researches on the analysis of the homogeneity of high-frequency heating through mathematical models are rarely involved.

Therefore, an accurate high-frequency heating and drying temperature field simulation model is established to analyze the factors affecting the heating uniformity in the wood drying process which can provide a scientific basis for the optimization of the process parameters in wood high-frequency vacuum drying and has crucial guiding significance for actual production. The primary contents of the article are as follows: 1) the simulation model of high heating temperature field based on finite element method is established and verified; 2) the influencing factors of high-frequency heating uniformity are analyzed; and 3) the process parameters are optimized.

MATERIALS AND METHODS

Model Development

According to the model construction principle of easy-to-difficult and simple-to-complex, at first, the model of only considering the high-frequency heating and thermoelectric coupling (temperature field simulation) of wood was built. Thereafter, the model of heat and mass transfer and stress–strain and wood anisotropy were gradually considered in the follow-up study.

To reasonably simplify the process of solving the high-frequency heating model, the following assumptions were made about the structure and properties of wood: 1) Only the heat transfer process is considered assuming that wood moisture level does not change. 2) The structural, physical, and chemical properties of wood are symmetrical, and the central layer is the adiabatic surface in the thickness direction. 3) Wood solid skeleton is rigid and does not shrink in the heating process. 4) The internal components of wood are inert and do not undergo any chemical changes during heating. 5) Compared with the whole drying process, high-frequency continuous heating time is relatively short; hence it is safe to assume that the thermal and electrical properties of wood are stable at the heating stage. 6) The upper, lower, and side surfaces of the stack have the same external environment, implying that the surface heat transfer coefficient is the same for all surfaces. 7) The external environment does not change with the wood heating, signifying that the parameters

such as surface heat transfer coefficient and ambient temperature are constant.

Geometric model. The finite element simulation software COMSOL5.2a (COMSOL Multiphysics, Burlington, VT) was used to simulate the high-frequency heating process. As shown in Fig 1, the geometric model of high-frequency heating was established according to the actual structure size of high-frequency vacuum drying device. The model structure consisted of a high-frequency vacuum drying tank (YASUJIMA Corporation, Ehime, Japan) (640 [diameter] × 1350 [depth] mm), parallel top and bottom plates (1000 × 400 × 1.3 mm), and heated timber (500 × 240 × 120 mm). The sample was placed at the geometric center of the upper and lower plates.

Governing equations. The electric field intensity and distribution in the heating process can be represented by Maxwell's equation (Alfaifi et al 2014) as follows:

$$-\nabla\cdot((\sigma+j2\pi\varepsilon_0\varepsilon')\nabla V)=0,$$

where σ is the electrical conductivity of wood ($S\cdot m^{-1}$), $j=\sqrt{-1}$, ε_0 is the vacuum dielectric constant, ε' is the dielectric constant of wood, and V is the electric potential across the electrode gap (V).

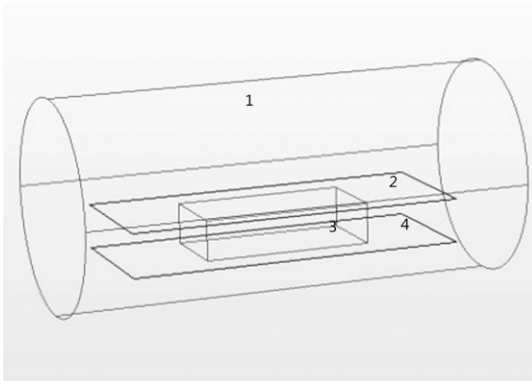

Figure 1. The geometric model of high-frequency heating (1. drying tank; 2. upper plate; 3. sample; 4. lower plate).

The heat conduction inside the piles is governed by Fourier formula as follows:

$$\frac{\partial T}{\partial t}=\alpha\nabla^2 T+\frac{P}{\rho c_p},$$

where $\partial T/\partial t$ is the instant heating rate in the stack ($°C\cdot S^{-1}$), α is the thermal diffusivity ($m^2\cdot s^{-1}$), ρ is the density ($kg\cdot m^{-3}$), C_p is the specific heat ($J\cdot kg^{-1}\cdot °C^{-1}$), and P is the power conversion in stack per unit volume ($W\cdot m^{-3}$).

The conversion of electromagnetic energy to thermal energy is represented by the following equation (Choi and Konrad 1991):

$$P=2\pi f\varepsilon_0\varepsilon''|E|^2,\ E=-\nabla V,$$

where f is the working frequency of the high-frequency equipment, ε'' is the loss factor of wood, and E is the electric field intensity in the stack.

Initial and boundary conditions. The high-frequency vacuum tank was set to be electrically insulated. The initial temperatures of all the structures were taken as room temperature (23°C) in the model. The heat transfer coefficient between wood and environment was taken as 12 W/(m^2°C) (Li et al 2008). The upper plate was set as the electromagnetic wave emitter and the lower plate was set as the ground electrode. The voltage between the upper and lower plates was considered to be uniformly distributed. At the same time, the voltage was also considered constant when the wood moisture was constant during high-frequency heating (Alfaifi et al 2014). The plate voltage was 1000 V (Liu et al 2014).

Table 1 shows the other characteristic parameters of the material involved in the model.

Simulation procedure. The joule heating module of the finite element simulation software (COMSOL5.2a) was selected to solve the coupling of electromagnetic wave heating and heat transfer equations. The software ran on workstations (Dell, Hopkinton, MA, dual-core 2GHz processor, 4 GB RAM, and Windows 8 64-bit operating system).

Table 1. The physical properties of the material in the model.

Physical properties	Pine	Air	Plate electrode	Tank
Density ($kg \cdot m^{-3}$)	616	1.2	2700	7850
Specific heat ($kJ \cdot kg^{-1} \cdot °C^{-1}$)	2104	1200	900	475
Thermal conductivity ($W \cdot m^{-1} \cdot °C^{-1}$)	0.1074	0.025	238	44.5
Dielectric constant	36	1	—	—
Loss factor	0.18	0	—	—

Model Validation

The Mongolian pine timber (*Pinus sylvestris* var. *mongholica* Litv.) with pith was used in the experiments to validate the model. The samples with no crack, decay, and deformation were selected and then processed into the size of 120 mm × 120 mm × 500 mm. The initial MC was measured to be 50% and the relevant physical parameters are shown in Table 1. The heating temperature of the test was set between 65 and 70°C. To satisfy assumption 1) of the section Model Development, the test sample was sealed with silica gel on its six surfaces and the pressure inside the vacuum tank was atmospheric pressure. As shown in Fig 2, the optical fiber temperature detection system (FISO Company, Toronto, Canadian, Type: I-EVO-040) was used to test the temperature (surface layer T_1, middle layer T_2, and core layer T_3) (T_3 was located at the center of the section, 60 mm from the top surface; T_2 was located directly above T_3, 40 mm from the top surface; T_1 was located directly above T_2, 20 mm from the top surface) of three parts in the thickness direction. The model was validated by comparing the detected value and simulation value at the same position of the stack. Each test was conducted on two samples and the samples were placed into the electrode plate side by side with a plate spacing of 130 mm and a plate area of 1000 × 400 mm. The experiments were repeated three times under the same conditions. When the center temperature of the sample reached the predetermined temperature, the test was considered over and the heating time and weight change of the test sample were recorded. Owing to a short heating time, the sample quality did not change by more than 0.5% (15-22g), as obtained through multiple measurements; therefore, the variation of wood moisture was ignored in the test process.

Heating Uniformity Evaluation

During the simulation, the temperature uniformity index (TUI) was estimated to evaluate the heating uniformity of the stack. The TUI can be used as an effective tool to evaluate the heating uniformity of the stack when using a fixed high-frequency heating device and specific high-frequency heating unit. TUI is defined as:

$$\mathrm{TUI} = \frac{\int_{V_{\mathrm{vol}}} |T - T_{\mathrm{ave}}| dV_{\mathrm{vol}}}{(T_{\mathrm{ave}} - T_{\mathrm{initial}}) V_{\mathrm{vol}}},$$

where V_{vol} is the volume of stack (m^3), T and T_{ave} represent the maximum temperature and the

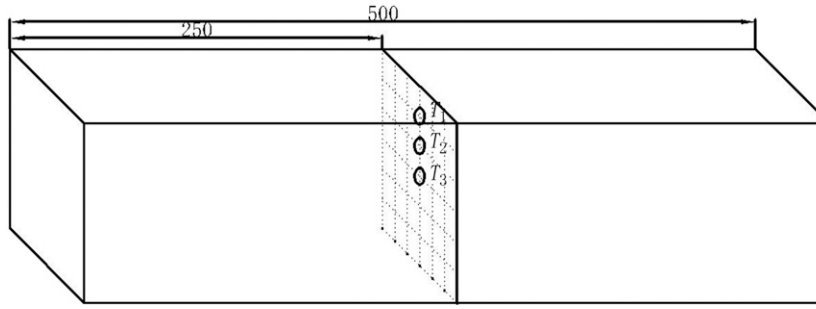

Figure 2. Test material and temperature measurement point (unit: mm); T_1: surface layer; T_2: middle layer; T_3: core layer.

average temperature of the stack (°C), respectively. The smaller the TUI, better the uniformity of high-frequency heating. The minimum value of TUI is zero, which indicates that the temperature distribution of the stack is uniform.

In the model, the stack size was taken as 500 × 240 × 120 mm and the electrode plate spacing (120, 130, 140, 150, and 160 mm), plate area (S_1 = 1200 × 500, S_2 = 1000 × 400, S_3 = 800 × 350, S_4 = 600 × 300, and S_5 = 500 × 240 mm), and the wood dielectric constant between plates [11, 9, 7, 5, and 3]]) were adjusted, respectively. Thereafter, the high-frequency continuous heating duration was set to 20 min and the change in TUI was analyzed. The plate area was S_2; when the stack width was 240 mm, the stack length was taken as 500, 600, 700, 800, 900, and 1000 mm. Also, when the stack length was 500 mm, the stack width was taken as 240, 280, 320, 360, and 400 mm. Then, high-frequency continuous heating for 20 min and analyzing the changes of TUI were carried out. When the plate spacing was 130 mm, the upper plate area was S_2 and the dielectric constant was 7 (the later stage of drying), adjusting the continuous heating time (30, 25, 20, 15, 10, 5, and 3 min) and then analyzing the effect of high-frequency application time on TUI change in the later stage of drying was carried out.

RESULTS AND ANALYSIS

Model Validation

Figure 3 shows the variation of the measured temperature at the measuring points of the surface layer, middle layer, and core layer of the test specimen after high-frequency continuous heating for 20 min. The temperature of the three measured points reached 57.2, 59.4, and 66.3°C, respectively, and increased exponentially in the initial stages of the experiment and then increased linearly after heating for 5 min. The measured temperatures were slightly lower than the simulated values in the early stages of the experiment and slightly higher than the simulated values in the later stages. According to the SPASS analysis, the correlation coefficients between the measured values of the three measuring points and the simulated values were 0.997, 0.997, and 0.998, respectively. The previous results demonstrate that the simulated temperature change was consistent with the measured temperature change, suggesting that the developed model has a high degree of accuracy and can be used for subsequent simulation studies.

Analysis of Stack Temperature Distribution

Figure 4 shows the simulated temperature distribution in the thickness direction (perpendicular to the electric field lines) and the length and width direction (parallel to the electric field lines) of the stack (500 × 240 × 120 mm), when the plate spacing was 130 mm and the area of the plate was S2 (1000 × 400 mm) after high-frequency heating for 20 min. In the direction of thickness, the temperature of the central layer (62-70°C) was the highest whereas those of the upper and lower surface (50-56°C, 50-55°C) were the lowest. This phenomenon can be explained via refraction and reflection of electromagnetic waves at the interface among the stack's upper and lower plates, and the tank body which resulted in

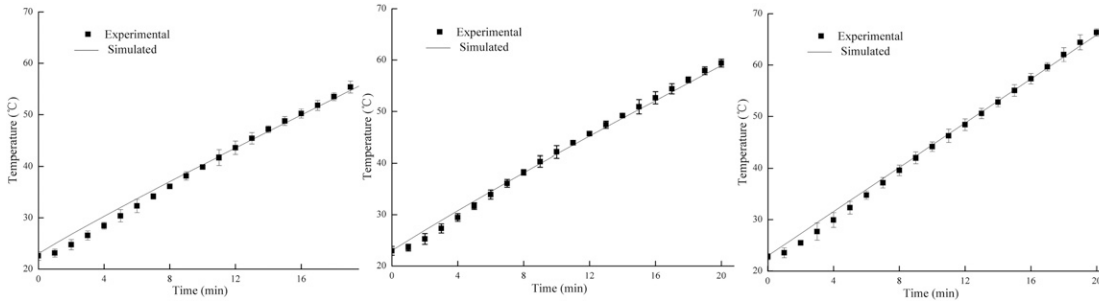

Figure 3. Experimental and simulated temperature of the measuring point (from left to right: surface layer, middle layer, and core layer).

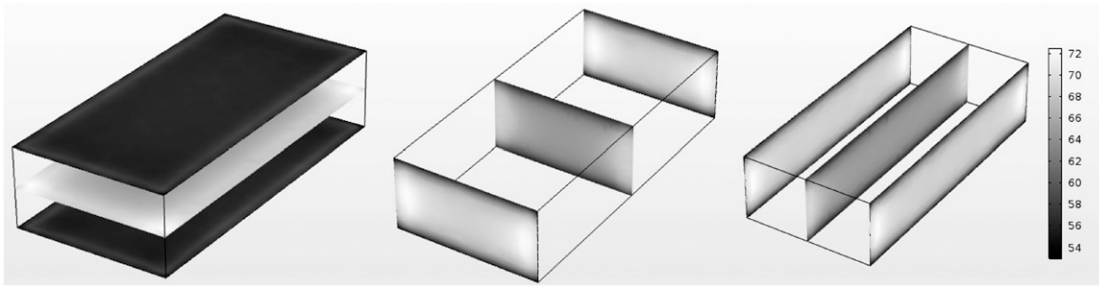

Figure 4. The stack temperature profile (unit: °C) (from left to right: thickness direction, length direction, and width direction).

concentration of more energy in the middle layer. In the longitudinal direction, the center temperature (53.5-65.4°C) was lower than the temperatures at both ends (50.7-68.6°C). This was due to the attenuation of energy and the edge effect of the electric field during the penetration of high-frequency electromagnetic waves (Huang et al 2015). Especially in the latter case, while stacking specimens between plates, the electric field lines bent inward near the edge of the plate and the degree of bending was higher closer to the edges. Hence, the electromagnetic field lines were relatively concentrated at the corners of the specimen, resulting in higher potential and temperature than in other regions. In the width direction, the temperature of the center layer was also lower than the temperature of both sides because of the same phenomenon.

Effect of Heating Uniformity on Plate Distance

Figure 5(a) shows the TUI of the stack (500 × 240 × 120 mm) at different plate spaces. The smaller the plate spacing, the lower the TUI, resulting in a better heating uniformity. For instance, when the plate spacing was the smallest (contacting the material and 120 mm), the TUI was the smallest at 0.128. The reason for the phenomenon is that the edge effect of the electric field between the electrode plates decreased as the plate spacing decreased. Although the contact between the test material and the plate led to the best heating uniformity, the grounding plate was connected to the wood support plate on the tank body. The heating loss of wood was caused by the conduction loss which led to a decrease in the wood temperature near the plate. During the actual drying process, the internally displaced water vapor would be condensed in the layer, resulting in an uneven distribution of the MC in the thickness direction. The improvement is to place a layer of dried and certain-thickness sheet (Simpson 2004) between the stack and the earth plate and leave no gaps among the wood, the dry sheet, and the plates.

Effect of Heating Uniformity on Plate Area

Figure 5(b) shows the TUI of the stack (500 × 240 × 120 mm) for plates of different areas. As the plate area increased, the TUI first decreased and then increased. When the plate area was S5 (500 × 240 mm) and the same for the horizontal cross-sectional area of the stack, the heating uniformity was the best. The reason for the phenomenon is that with the variation of the plate area, the electric field distribution of the pile changed (Huang et al 2015). When the plate area was too large, there was more serious electric field edge effect at the corner area of the pile. It was concluded that the uniformity was the best when the plate area and the horizontal cross-sectional area of the pile were the same.

Effect of Heating Uniformity on Dielectric Constant

Figure 5(c) shows the relationship between the heating uniformity and the dielectric constant of

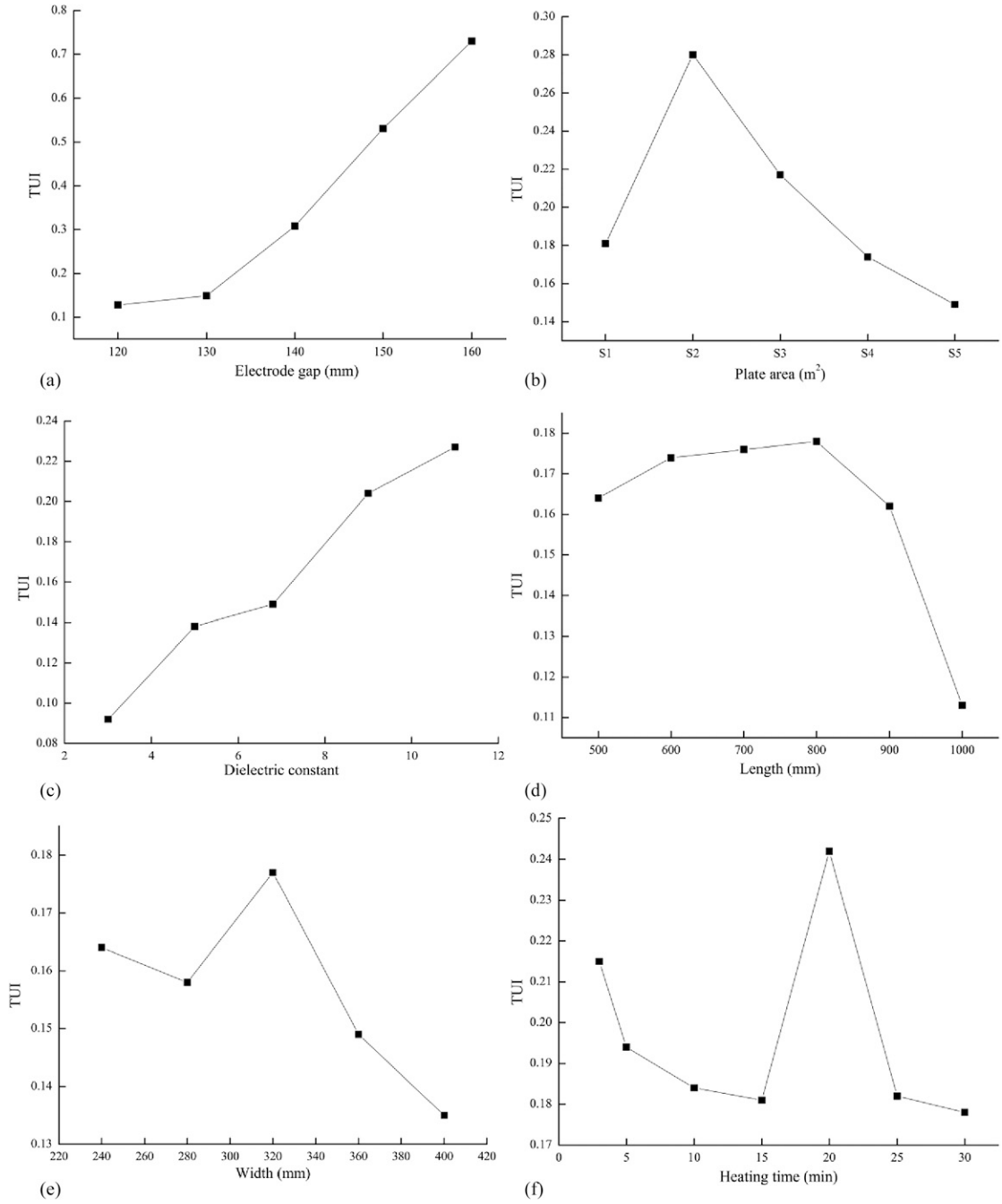

Figure 5. The temperature uniformity index (TUI) at different (a) electrode gaps, (b) plate areas, (c) dielectric constants, (d) stack lengths, (e) stack widths, and (f) heating times.

the sample. The results suggest that the smaller the dielectric constant, the better the heating uniformity. Because the dielectric constant and the MC of wood were approximately linear at the FSP, the smaller the water content, the smaller the TUI. The plausible reason remains to be studied further.

Effect of Heating Uniformity on Stack Length and Width

Figure 5(d) and (e) show the influence of the length and width of the stack on the heating uniformity when the area of the plate was S_2 (1000×400 mm) and the high-frequency heating was continued for 20 min. As the length of the wood pile increased, the TUI first increased and then decreased. When the length of the wood pile was the same as the length of the plate, the heating uniformity was the best. As the width of the wood pile increased, the TUI first decreased and then increased. As the width of the stack increased, the TUI first decreased, then increased, and then again decreased. The heating uniformity was the best when the width of the stack was consistent with the width of the plates. The reason for the phenomenon is the same as specified in the section Effect of Heating Uniformity on Plate Area. Based on the results presented in this section and section Effect of Heating Uniformity on Plate Area, the plate area should be compatible with the drying tank body and be as large as possible to increase the capacity factor of the equipment while the length and width of the pile should be consistent with the size of the plate to improve heating uniformity.

Effect of Heating Uniformity on Continuous Heating Time

Figure 5(f) shows the effect of high-frequency heating time on the heating uniformity of the stack under the conditions specified in section (Heating Uniformity Evaluation). During the course of continuous heating time, the TUI first decreased, then increased, and again decreased. During first 5 min, because of a short heating duration, the stack was not completely heated, and hence, there were more cold spots (Jiao et al 2014) resulting in relatively poor heating. During 5-15 min, the heating uniformity increased as the heating time increased. During 15-20 min, the dielectric relaxation frequency of the wood was lower than the high-frequency operating frequency which had a positive effect on the wood loss factor and temperature; hence, at higher temperatures, there was a stronger microwave absorption ability, which led to the "hot spots" phenomenon and reduced the heating uniformity (Li 2009; Lu et al 2015). During 20-30 min, the TUI decreased. This could be explained by the reason that the pile was exposed to high-frequency radiation for a long time and hence the cold spots of various parts were gradually eliminated. However, at this time, the temperature of the pile was extremely high, reaching more than 100°C, and some of the wood had been scorched and carbonized, which was not suitable for actual production.

CONCLUSION

In this article, a simulation model of wood high-frequency heating temperature field was constructed based on the finite element method. Through experimental verification, it was proved that the model was accurate and evaluating heating uniformity was feasible. The following conclusions were obtained through model analysis: 1) the temperature distribution of the stack: in thickness direction, the temperature of the middle layer was higher than the upper and lower surface temperatures; in the length and width direction, the center temperature was lower than those at both ends and both sides; and the temperature was the highest at the corners. 2) The influencing factors of heating uniformity: the heating uniformity increased with the decrease of plate space and the distance between the plates, and increased with the increase of the plate area. When the plate area was the same as the horizontal cross-sectional area of the stack, the heating uniformity was the best; the smaller the wood dielectric constant, the better the heating uniformity. As the continuous heating time

increased, the heating uniformity first decreased, then increased, and then again decreased. As the length and width of the stack increased, the heating uniformity decreased first, then increased, and then again decreased; when they were the same size as the plate, the heating uniformity was the best. 3) Optimization of process parameters: the plate area was adapted to the drying tank, as large as possible, to increase the capacity factor of the equipment; and the length and width of the stack should be consistent with the plate size to improve the heating uniformity; a layer of dried veneer was placed between the stack and plate to reduce drying defects, leaving no gaps among the wood, dry sheets, and plates.

ACKNOWLEDGMENT

This work was funded by the Chinese National Natural Science Foundation under Grant 31670562.

REFERENCES

Ai MY (2016) Practice and application of wood drying. Chemical Industry Press, Beijing, China. 311 pp.

Alfaifi B, Tang J, Jiao Y, Wang S, Rasco B, Jiao S, Sablani S (2014) Radio frequency disinfestation treatments for dried fruit: Model development and validation. J Food Eng 120(1):268-276.

Cai Y, Hayashi K, Sugimori M (2001) Three-dimensional measurement of temperature distribution in wood during radio-frequency/vacuum drying. Mokuzai Gakkaishi 47(5):389-396.

Choi CTM, Konrad A (1991) Finite element modeling of the RF heating process. IEEE Trans Magn 27(5):4227-4230.

Guo W, Fei BH, Chen EL (2009) Wood structural construction industry in China. China Wood Ind 23:19-22.

Huang R, Wu Y, Zhao Y, Lu J, Jiang J, Chen Z (2013) Factors affecting the temperature increasing rate in wood during radio-frequency heating. Dry Technol 31(2):246-252.

Huang Z, Zhu H, Yan R, Wang S (2015) Simulation and prediction of radio frequency heating in dry soybeans. Biosyst Eng 129:34-47.

Jia XR (2015) Radio frequency vacuum drying of square-edged timber with pith: Mathematical model and numerical analysis. PhD thesis, Northeast Forestry University, Harbin, IN. 33 pp.

Jiao Y, Tang J, Wang S (2014) A new strategy to improve heating uniformity of low moisture foods in radio frequency treatment for pathogen control. J Food Eng 141:128-138.

Lee NH, Li C, Zhao XF, Park MJ (2010) Effect of pre-treatment with high temperature and low humidity on drying time and prevention of checking during radio-frequency/vacuum drying of Japanese cedar pillar. J Wood Sci 56(1):19-24.

Li XJ (2009) Characteristics of microwave vacuum drying of wood and mechanism of thermal and mass transfer. China Environmental Science Press, Beijing, China. 65 pp.

Li XJ, Sun WS, Zhou T (2012) Mathematical modeling of temperature profiles in wood during microwave heating. Sci Sil Sin 48:117-121.

Li XJ, Zhang BG, Li WJ (2008) Mathematical modeling of wood microwave-vacuum drying. J Beijing For Univ 30(2):124-128.

Liu HH, Yang L, Cai Y, Hayashi K, Li K (2014) Distribution and variation of pressure and temperature in wood cross section during radio-frequency vacuum (RF/V) drying. BioResources 9(2):3064-3076.

Liu HH, Yang L, Wu ZH (2017) Effect of vacuum drying set and radio-frequency/vacuum drying on wood quality. Dongbei Linye Daxue Xuebao 45(2):61-64.

Lu J, Xu J, Wu Y (2015) Climatic signals in wood property variables of Picea crassifolia. Wood Fiber Sci 47(2): 131-140.

Lv YY, Fu ZY, Song TY (2015) The effect of radio-frequent heating on water migration for boxed-heart larch lumber. J Anhui Agric Sci 2:148-151.

Rabidin ZA, Seng GK, Wahab MJA (2017) Characteristics of Timbers Dried Using Kiln Drying and Radio Frequency-Vacuum Drying Systems. MATEC Web of Conferences. EDP Sciences 108: 10001.

Simpson WT (2004) Two-dimensional heat flow analysis applied to heat sterilization of ponderosa pine and douglas-fir square timbers. Wood Fiber Sci 36(3):459-464.

Wang Y (2013) Study on control method of high-frequency vacuum combined wood drying. MS thesis, Northeast Forestry University, Harbin, IN. 10 pp.

Xiao H (2009) Characteristics of heat and mass transfer in wood during radio-frequency vacuum drying. MS thesis, Northeast Forestry University, Harbin, IN. 31 pp.

Zhao JY, Fu ZY, Jia XR, Cai YC (2015a) Mathematical model to predict preheating time and temperature profile in boxed-heart square timber during preheating. Wood Fiber Sci 47(2):179-189.

Zhao JY, Fu ZY, Jia XR, Cai YC (2015b) Modeling conventional drying of wood: Inclusion of a moving evaporation interface. Dry Technol 34(5):530-538.